

UNCLASSIFIED



Australian Government
Department of Defence
Defence Science and
Technology Organisation

Transient Eddy-Current Nondestructive Evaluation: Benchmark Data for Backface Slots in a Plate

S K Burke and M E Ibrahim

Maritime Platforms Division
Defence Science and Technology Organisation

DSTO-TN-1047

ABSTRACT

The results of a benchmark experiment for transient eddy-current nondestructive evaluation are reported. The benchmark configuration corresponds to the canonical geometry of an air-cored probe coil positioned above a conductive plate containing a long back-face slot. The coil is excited by an exponentially-damped step function current and measurements are made of the change in the transient magnetic field due to the slot. The aim of the work is to provide experimental data for validation of theoretical models under development within the wider NDE community and to provide a common geometry against which the performance of a range of such models can be compared. A further aim of the work is to stimulate the ongoing development of quantitative methods in transient eddy-current research.

RELEASE LIMITATION

Approved for public release

UNCLASSIFIED

UNCLASSIFIED

Published by

*Maritime Platforms Division
DSTO Defence Science and Technology Organisation
506 Lorimer St
Fishermans Bend, Victoria 3207 Australia*

*Telephone: (03) 9626 7000
Fax: (03) 9626 7999*

*© Commonwealth of Australia 2011
AR-015-159
December 2011*

APPROVED FOR PUBLIC RELEASE

UNCLASSIFIED

UNCLASSIFIED

Transient Eddy-Current Nondestructive Evaluation: Benchmark Data for Backface Slots in a Plate

Executive Summary

Eddy-current testing (ET) is a well-established and reliable nondestructive evaluation (NDE) technique that is used extensively to ensure the structural integrity of military platforms. It relies on a time-varying magnetic field, produced by a probe coil, to induce eddy currents in a metallic component under test. The presence of defects such as fatigue cracks or corrosion perturb the local eddy-current distribution, leading to a change in the induced coil voltage, signaling the presence of a flaw.

The two principal variants of ET are distinguished by the time variation of the applied field. Conventional ET utilises an alternating current to excite a probe coil, and measurements are performed in the frequency domain. The emerging technique of transient eddy-current testing consists of time-domain measurements where the probe coil is excited by a pulsed current. Significant interest has been generated in the transient technique because of its potential advantages over conventional ET in circumstances such as the detection of buried defects in multi-layer metallic structures.

A range of mature numerical modelling packages can be used to predict the probe response and optimise inspection parameters for conventional ET. However, there is a distinct lack of such tools for transient eddy-current testing. Further development of the transient technique requires similar validated quantitative models to underpin probe design and inspection philosophy.

With this in mind, the aim of the present work is to provide high-quality experimental transient eddy-current data for a well-characterised benchmark configuration. These data will then be employed to validate numerical models, currently under development within the wider NDE community. The benchmark experiment also provides a common geometry against which the performance of a range of numerical models can be compared, and is expected to stimulate ongoing development of quantitative transient eddy-current methods.

The benchmark configuration is typical of the case where transient eddy-current NDE could be considered in preference to conventional eddy-current NDE. The experimental configuration and parameters for the benchmark problem are presented within the body of the report and, for ease of access, the transient magnetic field data are provided in electronic form in a series of files accompanying this report.

This work was initiated by the TTCP Technical Panel MAT-TP-5 *Nondestructive Evaluation for Asset Life Extension and Integrity* through the operating assignment TTCP MAT-TP-5 O33 'Transient Eddy-current Systems.'

UNCLASSIFIED

UNCLASSIFIED

This page is intentionally blank

UNCLASSIFIED

Contents

| | |
|--|----|
| 1. INTRODUCTION..... | 1 |
| 2. EXPERIMENT | 2 |
| 2.1 Probe and test specimens | 2 |
| 2.2 Experimental procedure..... | 2 |
| 2.3 Transient magnetic fields in absolute units | 5 |
| 3. RESULTS AND DISCUSSION | 6 |
| 4. CONCLUSION | 8 |
| APPENDIX A: DETERMINATION OF KEY PARAMETERS | 10 |
| A.1 Coil liftoff (h_1)..... | 10 |
| A.2 Position of the Hall-effect device (z_D) | 11 |
| A.3 Zero of time (t_0)..... | 14 |
| APPENDIX B: DATA FILES..... | 16 |

UNCLASSIFIED

This page is intentionally blank

UNCLASSIFIED

1. Introduction

Eddy-current Testing (ET) is a nondestructive evaluation (NDE) method used to ensure the structural integrity of air, land and maritime platforms. The technique is based on the induction of eddy-currents in the metallic component under test using a time-varying magnetic field produced by a small probe coil. The presence of defects such as fatigue cracks or corrosion perturb the eddy-current distribution in the vicinity of the defect. This perturbation leads to a change in the induced magnetic field and hence induced coil voltage that signals the presence of a flaw.

In conventional ET, an alternating current generally in the frequency range 100 Hz–1 MHz is used to excite the probe coil and the measurements are performed in the frequency domain. In transient eddy-current testing, measurements are performed in the time domain and the probe-coil is excited using a pulsed current. These complementary variants have their own particular strengths and weaknesses [1].

Similar to previous benchmark experiments for conventional (frequency-domain) ET, the purpose of the present work is to provide high-quality experimental transient (time-domain) eddy-current data for a well-characterised benchmark geometry [2, 3]. It is anticipated that these data will be used by the wider NDE community to test the capabilities of sophisticated theoretical models to predict the probe response for a generic hidden planar defect. The benchmark experiment also provides a common geometry against which the performance of a range of numerical models can be compared, and is expected to stimulate ongoing development of quantitative transient eddy-current methods.

The benchmark problem is that of transient eddy-current induction by a circular air-cored coil above a non-magnetic conductive plate containing a long, narrow, back-face slot of uniform depth and thickness. The coil is driven by an exponentially-damped square-wave current and the change in reflected magnetic field on the axis of the coil due to the presence of the slot is measured as a function of time.

The geometry selected for the benchmark problem was inspired by the practical inspection problem of eddy-current detection of a crack initiating and growing from the hidden (or back) face of a conductive plate. A planar defect (in this case, a narrow slot that simulates a crack) was selected, rather than a volumetric defect (such as a flat-bottom hole to simulate corrosion-induced loss of back-wall thickness) in order to provide a sufficient challenge for current theoretical models [4-6]. The problem is also one in which the transient technique would be considered preferable to conventional ET.

The experimental configuration and parameters for the benchmark problem are presented in Section 2 together with a description of the experimental procedure. The experimental results are discussed in Section 3 and, for ease of access, these data are also provided in electronic form in the series of files that accompany this report. For completeness, a detailed description of the methods used to determine some key experimental parameters is given in Appendix A.

2. Experiment

2.1 Probe and test specimens

A transient eddy-current probe (Figure 1) was fabricated at DSTO and consisted of an unshielded cylindrical air-cored coil and a linear ratiometric Hall-effect device (Honeywell IC RS 304-267) [7]. The probe parameters are given in Table 1. The Hall-effect device was oriented to measure B^z , the component of magnetic field* parallel to the axis of the coil. The coil was excited using an exponentially-damped square-wave current, which for present purposes can be expressed in the form [8, 9],

$$I(t) = I_{\infty}(1 - e^{-t/\tau})u(t) \quad (1)$$

where I_{∞} is the long-time (i.e., steady state) current, τ is the rise time of the excitation and $u(t)$ is the unit step function, $u(t) = 1$ for time $t > 0$ and zero otherwise. The current excitation parameters are given in Table 2.

The test specimens consisted of two Al-alloy test plates, F5 and F6. Each plate contained a wire-cut electro-discharge machined (EDM) slot across the entire width of the plate to simulate an idealised back-face crack (Figure 2). The electrical conductivity of the plates was determined using a Zetec MIZ-22 eddy-current test set operating at 240 kHz together with a set of eddy-current conductivity calibration standards. The plate and slot parameters are given in Table 3.

For reference, details on the determination of three of the key probe and current parameters are given in Appendix A; accurate measurement of the axial location z_D of the Hall-effect device provided the greatest challenge.

2.2 Experimental procedure

The experiments were performed using the TRECSCAN® transient eddy-current instrumentation controlled by ANDSCAN® software [10]. The output from the acquisition software in this case took the form of the transient magnetic field as a function of time, normalised to B_{∞}^z , the steady-state value of the magnetic field. In this way, the normalised z component of the magnetic field $B^z(t)$ measured by Hall-effect device is given by

$$B_{norm}^z(t) = B^z(t) / B_{\infty}^z \quad (2)$$

where B_{∞}^z is computed directly via the acquisition software from the transient waveform after allowing sufficient time for the initial transient response to decay [11].

* The generic term "magnetic field" is adopted throughout this report. To be strict, B^z refers to the "magnetic flux density".

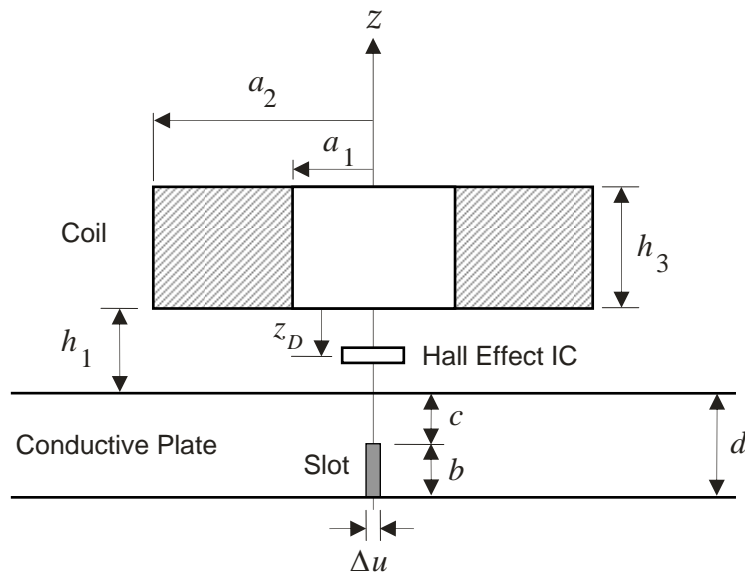


Figure 1 Schematic diagram of the experimental arrangement showing the cylindrical air-cored coil and Hall-effect device above a conductive plate containing a long back-face slot

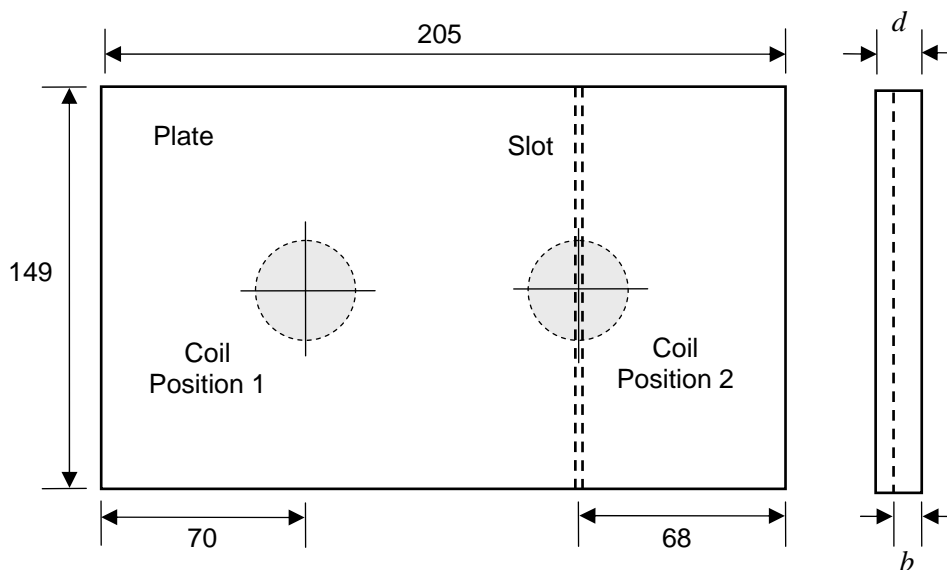


Figure 2 Test plate containing a long back-face slot (schematic). Transient eddy-current measurements were made with the coil at position 1 (over a defect-free region of the plate) and at position 2 (centred above the back-face slot). Measurements were also made with the plate removed (coil in air). All dimensions are in mm.

Table 1 Probe parameters (see Figure 1)

| | |
|---|-------|
| Inner radius a_1 (mm) | 8.72 |
| Outer radius a_2 (mm) | 15.50 |
| Length of windings h_3 (mm) | 6.88 |
| Number of turns N | 1008 |
| Isolated coil inductance L_0 (mH) | 23.13 |
| DC coil resistance R_0 (Ω) | 123 |
| Coil liftoff h_1 (mm) | 2.62 |
| Hall effect device offset [†] z_D (mm) | 1.8 |

Table 2 Coil current parameters: exponentially-damped square wave

| | |
|----------------------------|-----|
| Risetime τ (microsec) | 250 |
| Current I_∞ (mA) | 70 |
| Square-wave duration (ms) | 20 |

Table 3 Al-alloy test plates F5 and F6. Plate and Slot Parameters (see Figure 1)

| Plate Identification | F5 | F6 |
|---|-----------------|-----------------|
| Plate Thickness d (mm) | 6.45 | 6.45 |
| Conductivity σ (MS/m) | 22.8 | 22.8 |
| Resistivity ρ ($\mu\Omega\text{cm}$) | 4.38 | 4.38 |
| Magnetic Permeability μ_r | 1.00 | 1.00 |
| Ligament thickness c (mm) | 1.55 ± 0.05 | 1.09 ± 0.05 |
| Slot height b (mm) | 4.9 ± 0.05 | 5.36 ± 0.05 |
| Slot width Δu (mm) | 0.35 | 0.35 |

Measurements were made in three different probe configurations:

- (i) in the absence of the plate and remote from any conducting materials ('air measurement')
- (ii) on a defect-free region of the plate, i.e., position 1 shown in Figure 2 ('plate measurement'), and
- (iii) on the plate, centred above the back-face slot, i.e., position 2 shown in Figure 2 ('slot measurement').

These three measurements were then used to construct the following transient waveforms:

- (i) The normalised change in the reflected magnetic field due the defect-free plate,

$$\Delta B_{norm}^u(t) = B_{norm}^z(plate, t) - B_{norm}^z(air, t), \quad (3)$$

- (ii) The normalised change in the reflected magnetic field due to the back-face slot,

$$\Delta B_{norm}^c(t) = B_{norm}^z(slot, t) - B_{norm}^z(plate, t). \quad (4)$$

[†] Preferred value: for a full discussion on the systematic error in determination of z_D refer to Appendix A.

2.3 Transient magnetic fields in absolute units

For a benchmark experiment, it is preferable to provide the experimental magnetic field data in absolute units (in this case Tesla) rather than in normalised form. According to equations (2)-(4), it is possible to express the transient magnetic fields of interest in absolute units if B_∞^z is known.

With a knowledge of the probe and current parameters (Tables 1-2), it is straightforward to compute B_∞^z using the formula for the magnetic field on the axis of a cylindrical coil[‡] [9],

$$B_\infty^z = \frac{\mu_0 N I_\infty}{2(a_2 - a_1)h_3} \left[(h_3 + z_D) \log \left(\frac{a_2 + \sqrt{a_2^2 + (h_3 + z_D)^2}}{a_1 + \sqrt{a_1^2 + (h_3 + z_D)^2}} \right) - z_D \log \left(\frac{a_2 + \sqrt{a_2^2 + z_D^2}}{a_1 + \sqrt{a_1^2 + z_D^2}} \right) \right]. \quad (5)$$

Substituting the values from Tables 1-2 into Eq. (5), $B_\infty^z = 40.19 \text{ mTA}^{-1} \times 0.070\text{A}$, or

$$B_\infty^z = 2.81 \text{ mT} \quad (6)$$

for the present probe. Thus, from equations (2)-(4), the transient magnetic fields of interest can be expressed in absolute units as follows:

- The change in the reflected magnetic field due to the defect-free plate is

$$\Delta B^u(t) = B_{norm}^u(t) \times B_\infty^z, \quad (7)$$

- The change in the reflected magnetic field due to the back-face slot is

$$\Delta B^c(t) = B_{norm}^c(t) \times B_\infty^z, \quad (8)$$

where the scaling factor B_∞^z is given by Eq. (6).

[‡] There is a typographical error in [9] which is corrected here.

3. Results and Discussion

The results of the benchmark experiments are provided in the form of two ASCII files for specimens F5 ('F5Data.csv') and F6 ('F6Data.csv') accompanying this report. The data in these files consist of columns of comma separated values (csv) as follows:

time t (ms), ΔB_{norm}^u , ΔB_{norm}^c , ΔB^u (mT), ΔB^c (mT).

These data are given in both normalised and absolute forms so that any systematic experimental errors due to the scaling (Section 2.3) can be easily identified. For completeness, the results are tabulated for times t from 0 up to 20 ms but for all practical purposes the response has already decayed to zero for $t > 10$ ms (ΔB^c) and $t > 15$ ms (ΔB^u).

The transient magnetic field due to the plate $\Delta B^u(t)$ is plotted in Figure 3 together with the predicted theoretical response calculated using the parameters in Tables 1–3. As expected, there is little difference between the measured transients $\Delta B^u(t)$ for the defect-free regions of the two nominally identical plates. Theoretical calculations were performed using an in-house FORTRAN code which adopts a Fourier transform approach to obtain the time-domain response to an exponentially-damped square-wave excitation from the frequency-domain predictions of Dodd and Deeds [12]. This theoretical response is also provided in electronic form in the ASCII file 'CalculatedPlate.csv' which accompanies this report. The file again consists of data columns containing the comma separated values

time t (ms), ΔB_{norm}^u , ΔB^u (mT),

and which are given in both normalised and absolute format for $0 < t < 8$ ms.

The central results of this report are plotted in Figure 4, where the transient magnetic fields $\Delta B^c(t)$ due to a back-face slot in the Al-alloy specimens F5 and F6 are presented. The plot shows a number of interesting features. First, the response to the back-face slot in specimen F6 is larger than that for F5. This is because the slot size b for F6 is larger than that in F5 and is also closer to the front surface. Second, there is a small time delay before the transient response due to the slot develops. This is because at very short times the fields have not penetrated beyond the depth of the crack ligament so that the specimen appears to be defect-free at these short times. The delay is slightly shorter for F6 than F5 because the ligament length c for the slot in F6 (1.09 mm) is smaller than F5 (1.55 mm). Finally, the time at which the peak response is observed for F6 (0.72 ms) is earlier than for F5 (0.77 ms). This observation is consistent with the theoretical predictions of Fu and Bowler [4] who conclude that the peak time depends on the ligament length and is less sensitive to actual slot size, albeit for a slightly different geometry.

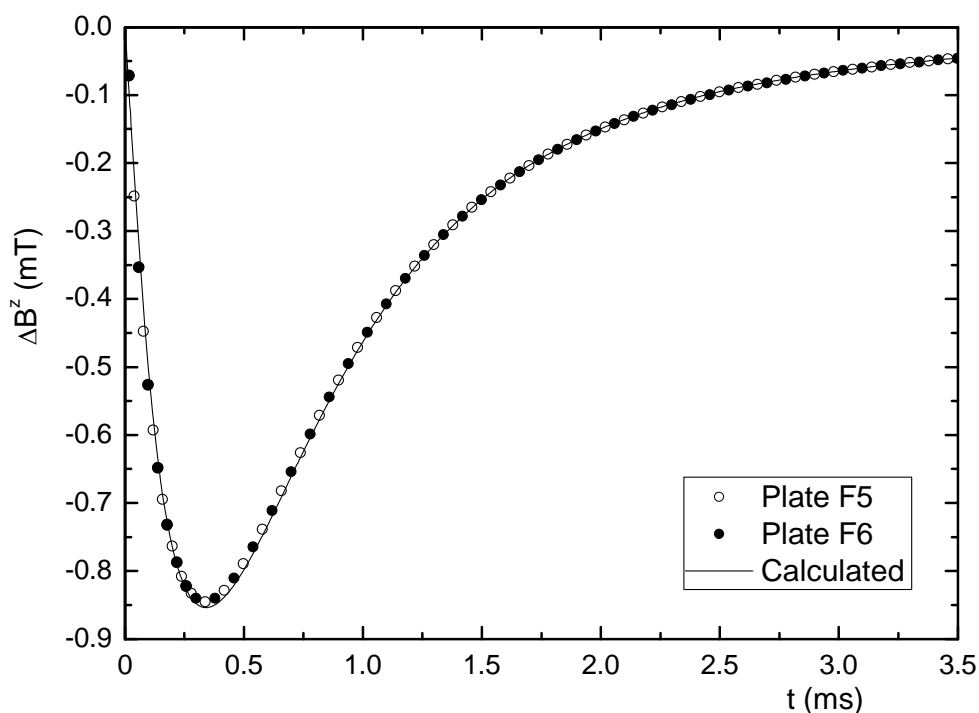


Figure 3 Transient magnetic field ΔB^u due to the defect-free region of plates F5 and F6. The points are the experimental results and the solid line is the calculated response. For clarity the experimental data for the two plates are interleaved and, for $t > 0.28\text{ms}$, only every fourth data point in each set is plotted.

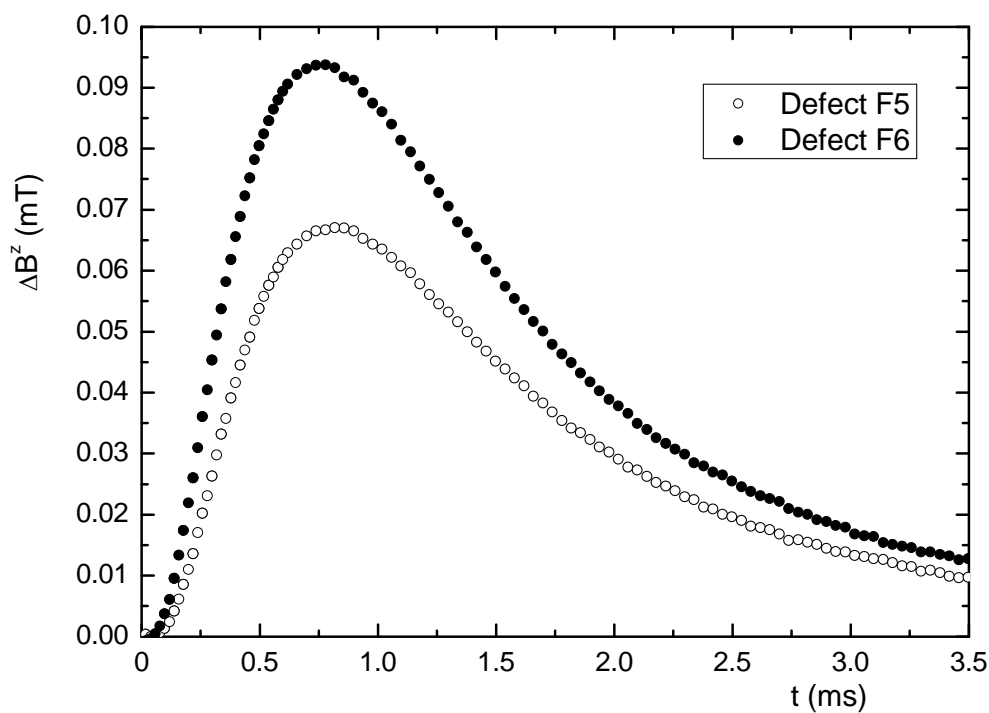


Figure 4 Transient magnetic field ΔB^c due to a back-face slot in Al-alloy plates F5 and F6. For $t > 0.6\text{ms}$, only every second data point is plotted to ensure clarity.

A number of improvements can be made in any future benchmark experiments of this type. First, as mentioned in Appendix A, the uncertainty in the measurements of the vertical location of the active area of the Hall-effect device should be reduced. In addition, Fu [5] makes the observation, based on theoretical calculations, that the transient response is highly sensitive to the coil location with respect to the slot, for example, an error of 2 mm in centring the large diameter coil above the slot can lead to a decrease in signal of some 10%. While an error of this magnitude is highly unlikely in the present experiments, the use of a precision scanning system in future would reduce the source of any such potential errors. Finally, in view of the computational burden associated with modelling open slots [4], it may be possible to reduce the slot opening somewhat below the current value of 0.35 mm through a systematic investigation of the EDM parameters such as feed-rate, wire diameter and spark gap.

4. Conclusion

A benchmark experiment for transient eddy-current NDE has been performed in which transient magnetic field data have been measured for a well-characterised canonical test geometry. The aim of the work is to provide experimental data for validation of theoretical models under development and to provide a common geometry against which the performance of a range of such models can be compared. A further aim of the work is to stimulate the wider development of quantitative methods in transient eddy-current NDE.

A future extension to this work would be to consider benchmark experiments involving narrow back-face slots of finite length and having either semi-elliptical or rectangular shape. The development and validation of models for such defects is a prerequisite for practical methods to determine the size, and hence the severity, of back-face cracks using transient eddy-current techniques.

Acknowledgements

The authors wish to thank Dr Geoff Hugo (DSTO) and Dr Robert Smith (QinetiQ, UK) for expert advice and guidance on the use of the TRECSCAN[®] system and Mr David Edgar (QinetiQ) for modifications to the ANDSCAN[®] software to suit the special requirements of these measurements. The authors are grateful to Dr John Bowler (CNDE, Iowa State University) for valuable discussions on the design of the benchmark experiments. We also wish to acknowledge the role of TTCP Technical Panel MAT-TP-5 in initiating this work through operating assignment TTCP MAT-TP-5 O30 "Transient Eddy-current Systems".

References

- [1] Smith RA and Hugo GR (2001), "Transient eddy current NDE for ageing aircraft - capabilities and limitations", *Insight* **43** 14-25.
- [2] Harrison DJ, Jones JD and Burke SK (1996), "Benchmark problems for defect size and shape determination in eddy-current nondestructive evaluation", *J. Nondestr. Eval.* **15** 21-34.
- [3] Burke SK (1988), "A benchmark problem for computation of ΔZ in eddy-current nondestructive evaluation (NDE)", *J. Nondestr. Eval.* **7** 35-41.
- [4] Fu F and Bowler JR (2006), "Transient eddy current response due to an open subsurface crack in a conductive plate" in *Review of Progress in Quantitative Nondestructive Evaluation Vol. 25*, edited by Thompson DO and Chimenti DE, CP820, (American Institute of Physics, New York), p. 337-344.
- [5] Fu F (2006), "Transient eddy current response due to a subsurface crack in a conductive plate", PhD Thesis, Iowa State University.
- [6] Bowler JR and Fu F (2004), "Transient eddy current interaction with an open crack" in *Review of Progress in Quantitative Nondestructive Evaluation Vol. 23*, edited by Thompson DO and Chimenti DE, CP700, (American Institute of Physics, New York), p. 329-335.
- [7] RadioSpares (2010), australia.rs-online.com, (Date accessed, August 2010).
- [8] Bowler JR and Harrison DJ (1992), "Measurement and calculation of transient eddy-currents in layered structures" in *Review of Progress in Quantitative Nondestructive Evaluation*; Vol. 11, edited by Thompson DO and Chimenti DE, (Plenum Press, New York), p. 241-248.
- [9] Bowler J and Johnson M (1997), "Pulsed eddy-current response to a conducting half-space", *IEEE Trans. Magn.* **33** 2258-2264.
- [10] QinetiQ (2011), www.andscan.com, (Date accessed, March 2011).
- [11] Johnson MJ and Bowler JR (1995), "Inversion of transient eddy-current signals for the determination of conducting plate parameters" in *Review of Progress in Quantitative Nondestructive Evaluation*; Vol. 14, edited by Thompson DO and Chimenti DE, (Plenum Press, New York), p. 849-856.
- [12] Dodd CV and Deeds WE (1968), "Analytical solutions to eddy-current probe-coil problems", *J. Appl. Phys.* **39** 2829-2838.
- [13] Burke SK (1992), "A semi-empirical model for eddy-current NDE using ferrite-cored probes", *Nondestr. Test. Eval.* **6** 267-277.
- [14] Smythe WR (1968), *Static and dynamic electricity*, 3rd ed. p. 297 (McGraw-Hill, New York).

Appendix A: Determination of Key Parameters

This Appendix contains a detailed description of the methods used to determine three of the key parameters in the benchmark experiments and is provided for reference purposes. The method used to determine the coil liftoff h_1 is given in subsection A.1, the approach used to estimate z_D , the vertical position of the active area of the Hall-effect IC, is described in subsection A.2 and measurement of the zero-of-time is discussed in subsection A.3.

A.1 Coil liftoff (h_1)

The coil liftoff h_1 given in Table 1 was obtained from frequency-domain measurements of the normalised coil impedance change for a separate, large Al-alloy block that approximated a conductive half-space [2]. With the other coil parameters fixed, the theoretical coil liftoff was varied to obtain the best fit between the calculated and experimental frequency variation of the coil impedance when plotted in the normalised impedance plane (Figure A1). The calculations were performed using the theory of Dodd and Deeds [12]. The best fit was found for $h_1 = 2.62$ mm, which is in reasonable agreement with the nominal value of 2.5 mm. Note that these measurements are of the coil impedance alone and do not involve the Hall-effect device at all.

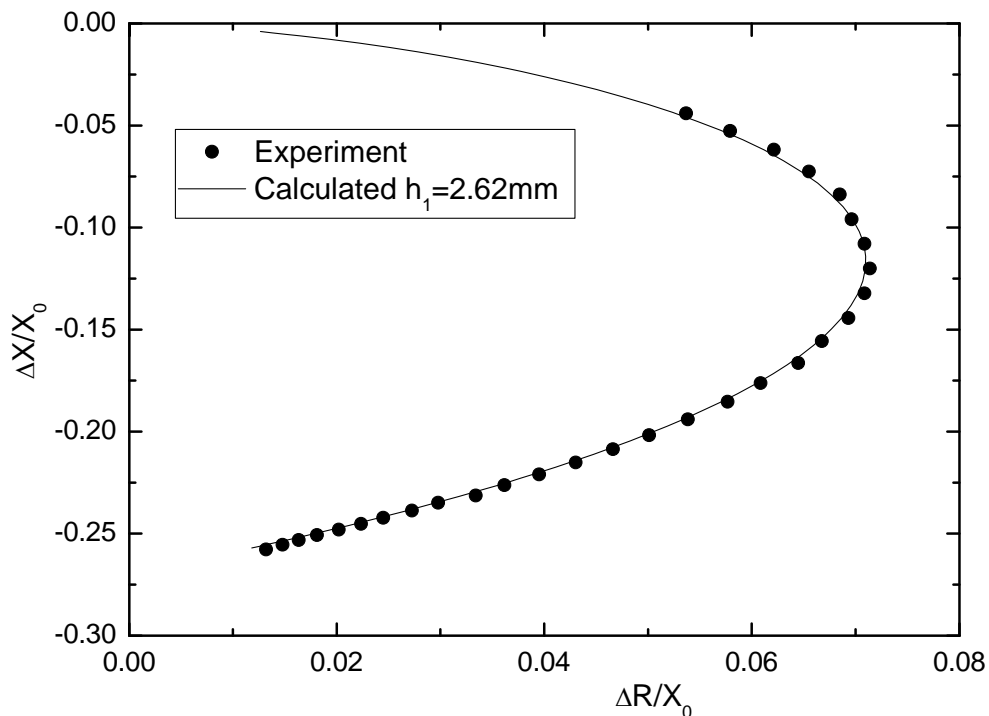


Figure A1 Determination of coil liftoff. The theoretical coil liftoff was varied to obtain the best fit between the calculated and experimental frequency variation of the coil impedance when plotted in the normalized impedance plane. The best fit by eye (solid line) was obtained for a liftoff $h_1 = 2.62$ mm with an uncertainty of approximately ± 0.02 mm.

A.2 Position of the Hall-effect device (z_D)

The most challenging parameter to measure was the location of the active area of the Hall-effect device with respect to the coil windings (z_D in Figure 1) once the probe had been assembled.

Direct measurement of the relative distances is difficult because of uncertainty in estimating the exact location of the active area of the device within the moulded packaging of the chip. Thus, following a similar philosophy to Harrison *et al.* [2], a method based on electromagnetic measurements was used to determine z_D . Two approaches were adopted, both of which were based on comparing frequency-domain measurements of the magnetic field detected by the Hall-effect device with the theoretical predictions. The first approach relied on estimating z_D from the magnitude of the magnetic field with the probe assembly in air. The second approach sought to determine z_D by comparison with theoretical predictions for the probe above a defect-free region of the plate.

The AC measurements were carried out using an HP-4192A Impedance Analyzer operating in gain-phase mode using the circuit shown schematically in Figure A.2. In this configuration, the magnitude and phase of the output of the Hall-effect IC is measured relative to coil current.

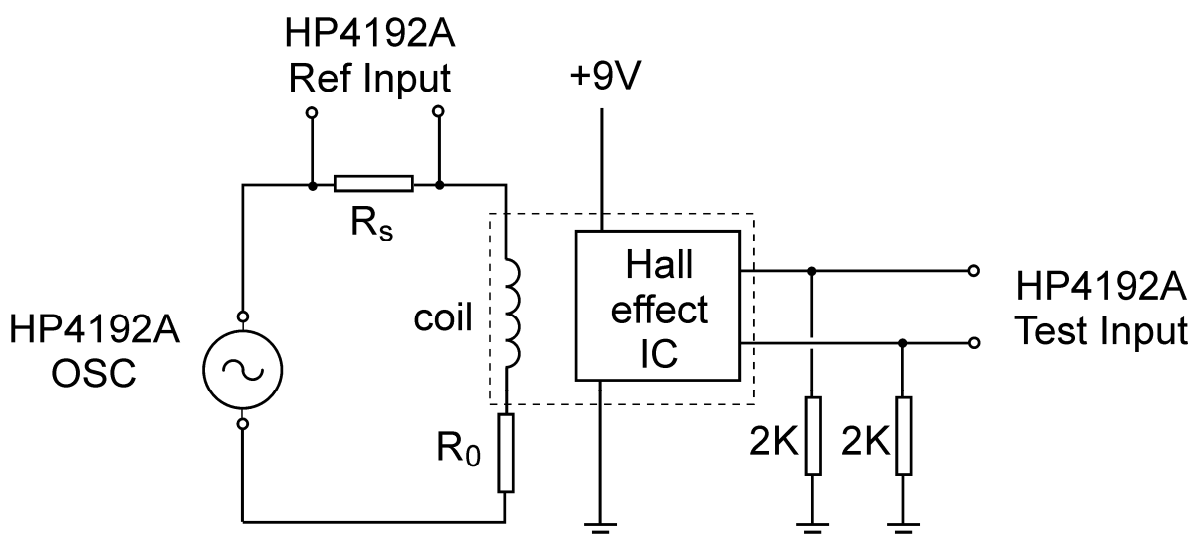


Figure A2 AC magnetic field measurement using the probe Hall-effect IC and HP-4192A Impedance Analyzer in gain-phase mode (schematic). The voltage across the standard resistor ($R_s = 47\Omega$) is proportional to the coil (probe coil or solenoid) current and is used as the reference input. The test input is the output from the Hall-effect IC. When calibrated, this configuration measures the magnitude and phase of the Hall-effect magnetic field per unit coil current. For completeness, the series resistance of the coil has been included, denoted R_0 .

Before proceeding with this plan, the Hall-effect device required calibration in order that the AC gain measured by the HP-4192A could be converted to magnetic field per unit current, B^z/I . The calibration was carried out by placing the entire probe assembly coaxially in a long single-layer solenoid having well defined geometry and hence a known axial magnetic field [13]. The geometry is shown in Figure A3, where at a position O the axial component of magnetic flux density per unit driving current is given by the expression [14]

$$B^z/I = \frac{1}{2} \mu_0 n_L (\cos \beta_2 - \cos \beta_1), \quad (\text{A1})$$

where $n_L = N/L$ is the number of turns per unit length of the solenoid and I is the solenoid driving current. With the Hall-effect device situated midway along the solenoid, $\beta_2 = 180 - \beta_1$, $\cos \beta_2 = -\cos \beta_1$ and hence from Eq. (A1)

$$B^z/I = \mu_0 n_L \frac{L/2}{\sqrt{(L/2)^2 + a^2}}. \quad (\text{A2})$$

With the measured solenoid parameters $N = 570$, $L = 131$ mm and $a = 21.47$ mm, the solenoid factor calculated using Eq.(A2) for calibration in this case is 5.19 mT/A. The results of the system calibration are shown in Figure A4.

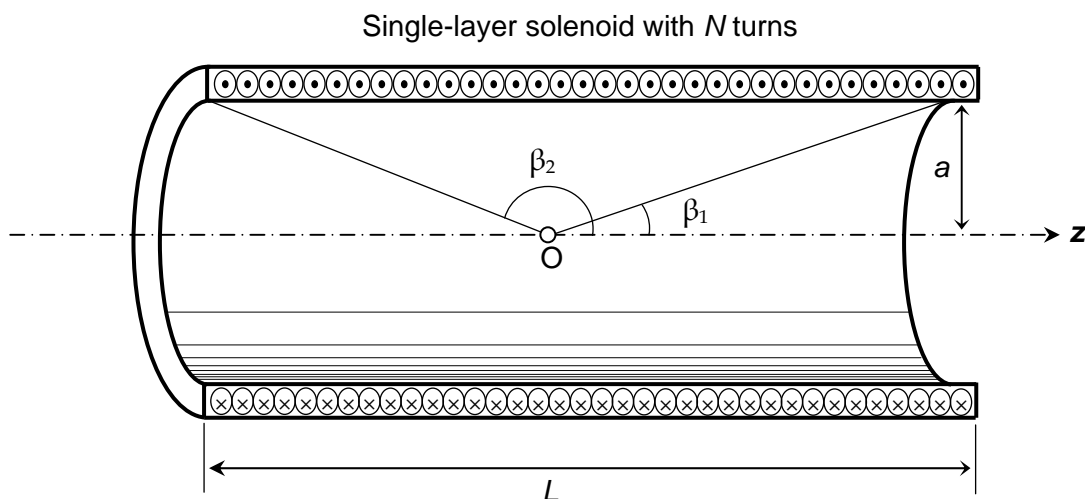


Figure A3 Schematic diagram showing the geometry of the single layer solenoid used for frequency-domain calibration of the probe Hall-effect device

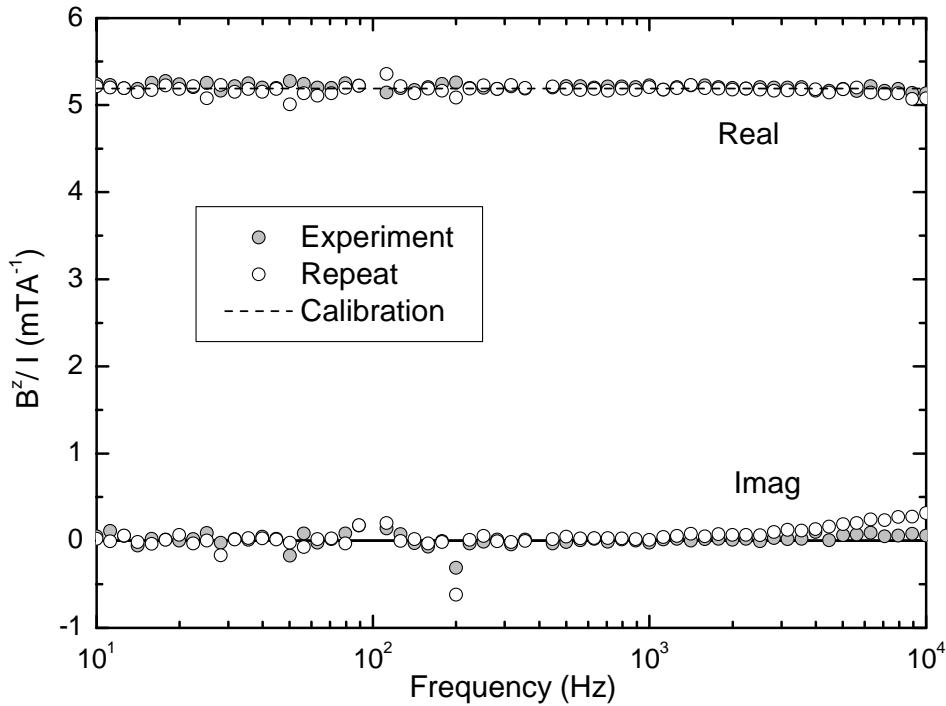


Figure A4 System calibration results. Frequency variation of the measured magnetic field per unit current with the probe centred within the single-layer solenoid. The dashed line represents the value of 5.19 mTA^{-1} required for correct calibration. For the probe in air, the magnetic field is expected to be purely real (i.e. in phase with the driving current) and the imaginary (out-of-phase) component zero. Experimental results are shown for two separate measurements to indicate the degree of scatter.

Having calibrated the system as described, measurements could then be made of the axial magnetic field per unit coil current $\text{Re}[B^z(\omega)/I]$ with the probe in air. The resulting value over the frequency range 10 Hz–10 kHz, averaged over three determinations, was 41.2 mTA^{-1} . For a cylindrical air-cored coil, the theoretical value of $\text{Re}[B^z(\omega)/I]$ measured on the coil axis is given by the expression, cf. Eq. (5),

$$\text{Re}[B^z/I] = \frac{\mu_0 N}{2(a_2 - a_1)h_3} \left[(h_3 + z_D) \log \left(\frac{a_2 + \sqrt{a_2^2 + (h_3 + z_D)^2}}{a_1 + \sqrt{a_1^2 + (h_3 + z_D)^2}} \right) - z_D \log \left(\frac{a_2 + \sqrt{a_2^2 + z_D^2}}{a_1 + \sqrt{a_1^2 + z_D^2}} \right) \right]. \quad \text{A3}$$

Using the coil dimensions in Table 1, a value of 41.2 mTA^{-1} is obtained from Eq. A3 for a value $z_D = 1.5 \text{ mm}$.

A second independent estimate for z_D was then obtained from measurements of the change in the magnetic field due to the plate per unit current as a function of frequency $\Delta B^z(\omega)/I$, by subtracting the probe response in air from the response with the probe on a defect-free region of the Al alloy plates (coil position 1 in Figure 2). Using the known coil

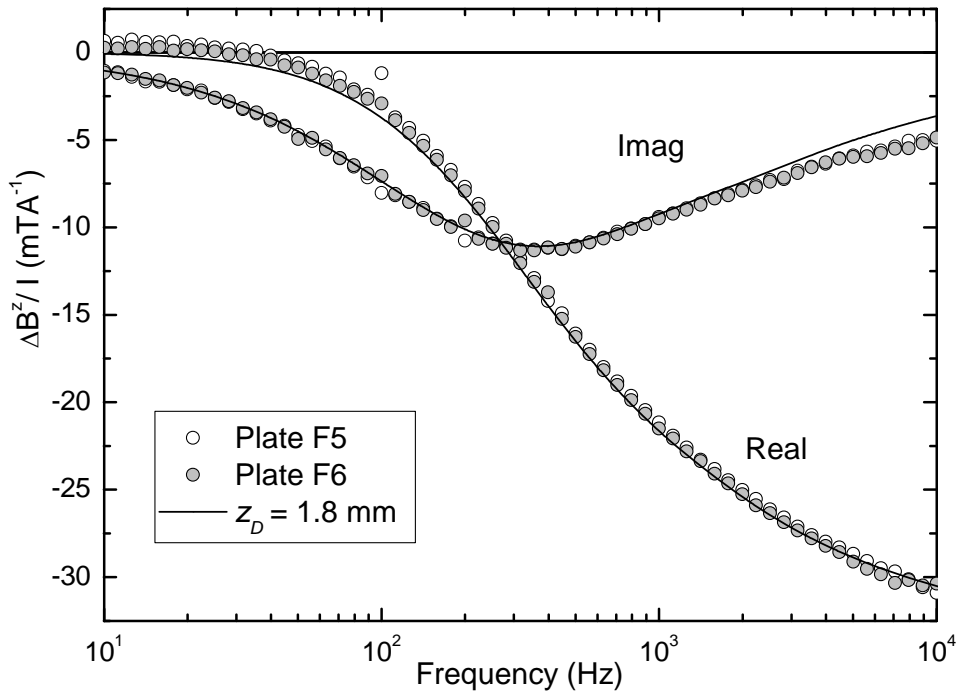


Figure A5 Frequency domain measurements to determine z_D . The change in magnetic field due to eddy-current induction in defect-free regions of the plates F5 (open symbols) and F6 (solid symbols) is compared with the theoretical predictions obtained for $z_D=1.8$ m.

parameters, known coil liftoff from Section A.1 and known plate conductivity, the value of z_D was varied to obtain the best agreement between the theory of Dodd and Deeds [12] and experimental data (Figure A5). This procedure resulted in the estimated value $z_D = 1.8$ mm.

Thus, according to these two electromagnetic measurements, z_D lies in the range 1.5 – 1.8 mm. A direct length measurement using Vernier callipers prior to final assembly of the probe resulted in an estimated z_D value of 1.6 mm. The preferred value, given in Table 1, is 1.8 mm as this value results in the best agreement between theory and experiment for the reflected transient field due to the defect-free plate (Figure 3). The consistency and accuracy in determining z_D was less than expected and alternative strategies for more precise measurement of z_D are a clear area of potential improvement in any subsequent benchmark experiments.

A.3 Zero of time (t_0)

The ‘zero of time’ for the transient measurements was obtained by fitting the normalised transient response of the probe in air to a function of the form

$$B_{norm}^z(t) = A(1 - \exp[-\frac{(t_0 - t)}{\tau}]) - Ct \quad (\text{A4})$$

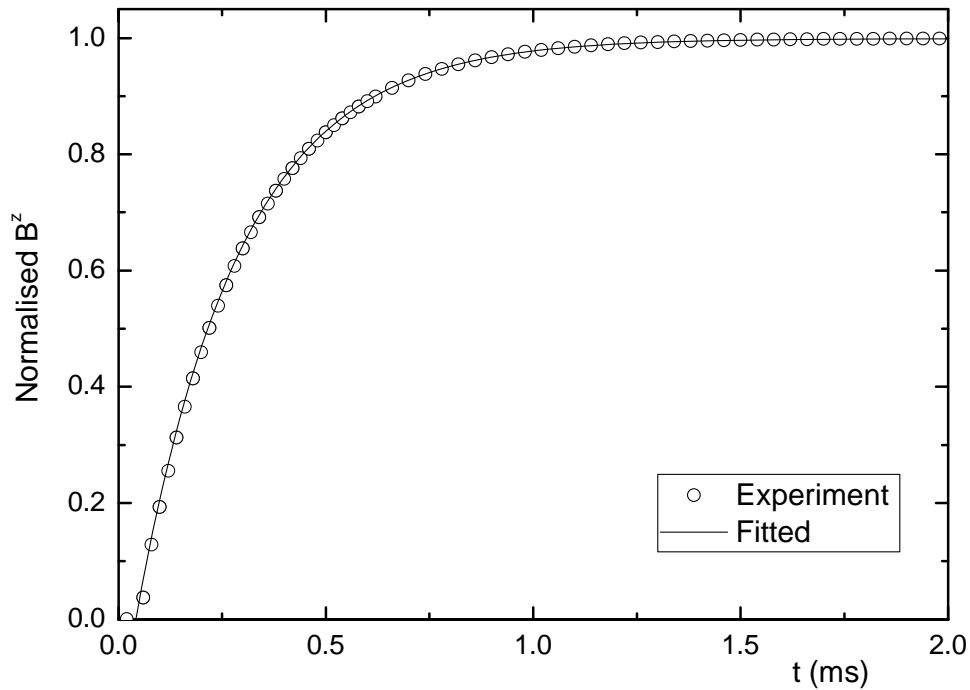


Figure A6 Transient magnetic field for the probe in air, uncorrected for t_0 . Experimental data (points) are compared with the results of a least-squares fit to the function in Eq. (5) for an early-time portion of the waveform. The fitted parameters in this case were: $A = 1.0000$, $t_0 = 0.04202$ ms and $C = 0.00051$ s⁻¹. For $t > 0.6$ ms, only every second data point is plotted to ensure clarity.

where the time constant $\tau = 250$ μ s is fixed and A , t_0 and C are the unknown parameters. A comparison between the experimental results and the theoretical predictions is shown in Figure A6. The “zero of time” t_0 obtained in this way did not vary significantly for the experimental trials and the same value $t_0 = 0.042$ ms was used to set $t = 0$ in the time scale for all of the benchmark data sets. Note that a very small linear term Ct was included in the fits but can be ignored in the theoretical analysis.

Appendix B: Data files

This Appendix contains the links to the ASCII files containing the benchmark data.

[DSTO-TN-1047 F5Data.csv](#)

[DSTO-TN-1047 F6Data.csv](#)

[DSTO-TN-1047 Calculated Plate.csv](#)

| | | | | | |
|---|--|-----------------------------------|---|---|--|
| DEFENCE SCIENCE AND TECHNOLOGY ORGANISATION DOCUMENT CONTROL DATA | | | | 1. PRIVACY MARKING/CAVEAT (OF DOCUMENT) | |
| | | | | | |
| 2. TITLE Transient Eddy-Current Nondestructive Evaluation: Benchmark Data for Backface Slots in a Plate | | | 3. SECURITY CLASSIFICATION (FOR UNCLASSIFIED REPORTS THAT ARE LIMITED RELEASE USE (L) NEXT TO DOCUMENT CLASSIFICATION) Document (U) Title (U) Abstract (U) | | |
| 4. AUTHOR(S) S K Burke and M E Ibrahim | | | 5. CORPORATE AUTHOR DSTO Defence Science and Technology Organisation 506 Lorimer St Fishermans Bend Victoria 3207 Australia | | |
| 6a. DSTO NUMBER DSTO-TN-1047 | | 6b. AR NUMBER AR-015-159 | | 7. DOCUMENT DATE December 2011 | |
| 6c. TYPE OF REPORT Technical Note | | 7. DOCUMENT DATE December 2011 | | | |
| 8. FILE NUMBER 2011/1081004/1 | | 9. TASK NUMBER ERP 07/368 | | 10. TASK SPONSOR CMPD | |
| 11. NO. OF PAGES 16 | | 12. NO. OF REFERENCES 14 | | | |
| 13. URL on the World Wide Web http://dspace-dsto.dsto.defence.gov.au/dspace/ | | | 14. RELEASE AUTHORITY Chief, Maritime Platforms Division | | |
| 15. SECONDARY RELEASE STATEMENT OF THIS DOCUMENT <i>Approved for public release</i> | | | | | |
| OVERSEAS ENQUIRIES OUTSIDE STATED LIMITATIONS SHOULD BE REFERRED THROUGH DOCUMENT EXCHANGE, PO BOX 1500, EDINBURGH, SA 5111 | | | | | |
| 16. DELIBERATE ANNOUNCEMENT No Limitations | | | | | |
| 17. CITATION IN OTHER DOCUMENTS Yes | | | | | |
| 18. DSTO RESEARCH LIBRARY THESAURUS http://web-vic.dsto.defence.gov.au/workareas/library/resources/dsto_thesaurus.shtml Non-destructive testing, Electromagnetic Induction, Magnetic Fields, Magnetic Measurement | | | | | |
| 19. ABSTRACT The results of a benchmark experiment for transient eddy-current nondestructive evaluation are reported. The benchmark configuration corresponds to the canonical geometry of an air-cored probe coil positioned above a conductive plate containing a long back-face slot. The coil is excited by an exponentially-damped step function current and measurements are made of the change in the transient magnetic field due to the slot. The aim of the work is to provide experimental data for validation of theoretical models under development within the wider NDE community and to provide a common geometry against which the performance of a range of such models can be compared. A further aim of the work is to stimulate the ongoing development of quantitative methods in transient eddy-current research. | | | | | |